American Mineralogist, Volume 94, pages 1333–1340, 2009

Structural and spectroscopic characterization of a suite of fibrous amphiboles with high environmental and health relevance from Biancavilla (Sicily, Italy)

Giovanni B. Andreozzi, Paolo Ballirano, Antonio Gianfagna, Simona Mazziotti-Tagliani, and Alessandro Pacella*

Dipartimento di Scienze della Terra, Sapienza Università di Roma, Piazzale Aldo Moro, 5-I-00185 Roma, Italy

Abstract

This study reports new spectroscopic and structural data of fibrous amphiboles from the volcanic area of Biancavilla (Sicily, Italy) that generated interest because of an anomalous increase of pleural mesothelioma of inhabitants. Each of the four samples is made of loose fibers, which show an edenite-winchite (fluorine) compositional trend, with significant tremolite component. Small amounts of iron (3.6–6.0 wt% FeO_{tot}) were identified in all samples, and the Fe^{3+}/Fe_{tot} ratios were evaluated by Mössbauer spectroscopy: two samples are characterized by Fe^{3+}/Fe_{tot} ratios between 50 and 70%, and the other two have Fe^{3+}/Fe_{tot} ratios higher than 90%. The OH-stretching region was investigated by FTIR, and no absorption bands were observed. Structural investigation was carried out by X-ray powder diffraction using the Rietveld method. Cell parameters, positional parameters for all the atoms, and site scattering for M1, M2, M3, M4, A, and A(*m*) were refined. The most important differences with respect to prismatic fluoro-edenite are the decrease of β, *a*, and *c* with decreasing Ca content, A-site occupancy, and tetrahedral Al content, respectively. By combining chemical, spectroscopic, and structural data, possible site occupancies were obtained. In particular, it was found that Fe^{2+} is distributed between M1 and M2 sites; moreover, for the two samples enriched in Fe^{2+}, it is also present at M4. Fe^{3+} is generally ordered at M2 site; however, for the two samples enriched in Fe^{3+}, minor amounts are partially disordered between M1 and M3 sites.

For the Biancavilla amphibole fibers, the large compositional variation observed in every sample makes the classification very difficult, so that the regulatory agencies would not classify as "asbestos" the whole mineral series, because of the large components of edenite and winchite in addition to tremolite. Many common features were found with respect to amphibole fibers from Libby, Montana, including Fe contents and oxidation state. Preliminary results of in vitro toxicological tests on Biancavilla fibers confirmed their high reactivity, and suggest that the samples with the highest Fe^{2+} contents induce a rapid start to cell mortality.

Keywords: Amphiboles fibers, fluoro-edenite, Biancavilla, Mössbauer spectroscopy, Rietveld method, crystal chemistry, environmental and health relevance

Introduction

The quantitative characterization of mineral fibers, and in particular of amphiboles fibers, is a topical subject due to environmental and health concerns. An interesting starting point to both clarify the classification of mineral fibers (asbestos or not) and enhance our understanding of fiber-lung reactivity mechanisms is the case study of Biancavilla (Sicily, Italy). In this area, in fact, the presence of some unexpected cases of pleural mesothelioma in local inhabitants (Paoletti et al. 2000) was correlated to the widespread occurrence of amphibole fibers (Comba et al. 2003; Burragato et al. 2005). A new amphibole species, fluoro-edenite, was recognized in volcanic products, and loose fibers of amphibole were retrieved in the lungs of people who had died from pleural mesothelioma. Recent studies on the reactivity of these amphibole fibers in organic environments showed that their toxicity is strongly related to differences in composition, in particular Fe content and oxidation state (Soffritti et al. 2004; Cardile et al. 2004; Pugnaloni et al. 2007).

The mineralogical literature reports few works dealing with quantitative chemistry of fibrous minerals. Recently, Meeker et al. (2003), Gunter et al. (2003, 2007), Pacella et al. (2008), and Ballirano et al. (2008) reported good attempts to realize this goal for fibrous amphiboles (e.g., winchite, tremolite), using specific analytical procedures. Qualitative chemical studies on Biancavilla loose fibers were reported in Gianfagna et al. (2003) and Bruni et al. (2006) and display compositional differences between fibrous samples and prismatic fluoro-edenite. A first attempt to obtain the full characterization of a sample of loose fibers from Biancavilla was reported in Gianfagna et al. (2007): the semi-quantitative chemical characterization of the sample (from the Poggio Mottese locality) was obtained exploiting a SEM-EDS "overlapping" analytical method. However, the method was further improved and tested on different types of fibrous amphiboles in Paoletti et al. (2008). Finally, a detailed quantitative chemical characterization of a suite of four fibrous samples from Biancavilla was reported in Mazziotti-Tagliani et

* E-mail: alessandro.pacella@uniroma1.it

0003-004X/09/0010–1333$05.00/DOI: 10.2138/am.2009.3214

al. (2009), together with hypotheses about fiber genesis.

In the present work, the full structural and spectroscopic characterization of the same four samples chemically characterized in Mazziotti-Tagliani et al. (2009) has been performed. Cation site partitioning has been obtained by optimizing average chemical, Mössbauer, FTIR, and X-ray powder diffraction data.

Materials and analytical methods

The samples studied come from four distinct localities around Biancavilla town. The starting materials were enriched, so the final mineral assemblages are made of loose fibers of amphiboles and accessory feldspars of micrometrical and sub-micrometrical dimensions.

Fourier transform infrared spectroscopy

Fourier transform infrared (FTIR) spectroscopic data were collected using a Perkin Elmer spectrometer (SYSTEM 2000) in the range 4000–400 cm^{-1}: 32 scans at a nominal resolution of 4 cm^{-1} were averaged. The instrument was equipped with a KBr beamsplitter and TGS detector. The samples were ground in an agate mortar and mixed in a 2:100 ratio with 200 mg of KBr to obtain transparent pellets. Measurements were done in air at room temperature. For all spectra, no absorption bands were observed in the OH-stretching region (3800–3600 cm^{-1}), as already verified for the prismatic fluoro-edenite (Gianfagna and Oberti 2001).

^{57}Fe Mössbauer spectroscopy

All samples were gently ground in an agate mortar with acetone and mixed with powdered acrylic resin to avoid (or reduce) preferred orientation. Depending on the availability of material, between 10 to 70 mg of sample were pressed to make an absorber within the limits of the thin absorber described by Long et al. (1983). The spectra were collected at room temperature using a conventional spectrometer operating in costant acceleration mode, with a ^{57}Co source of nominal strength of 50 mCi in a rhodium matrix. The data were recorded using a multichannel analyzer using 512 channels for the velocity range from –4 to 4 mm/s. To obtain good statistical counting, about 10^7 counts per channel were collected. After velocity calibration against a spectrum of high-purity α-iron (25 μm thick), the raw data were folded to 256 channels. The spectra were fitted using the Recoil 1.04 fitting program (Lagarec and Rancourt 1998). A first cycle of refinement was performed by fitting three doublets, pure Lorentzian line-shapes (spectra and hyperfine parameters not reported but available on request), and the results obtained were quite satisfactory (χ^2 always <1), but the Lorentian line-shapes showed, in some cases, wide line-widths (Γ values up to 0.92 mm/s). Therefore, a second cycle of refinement was carried out by fitting quadrupole-splitting distribution (QSD), following the approach of Gunter et al. (2003) and Gianfagna et al. (2007). Several fitting models with unconstrained parameters [isomer shift (δ_0), coupling parameter (δ_1), center of Gaussian component (Δ_0), Gaussian width (σ_Δ), and absorption area (A)] were tried to obtain the best fit. A model based on two sites ($1Fe^{2+}$ + $1Fe^{3+}$), each with two components, was finally chosen and the results were very satisfactory (Table 1; Fig. 1). Increasing the number of Gaussian components did not significantly change the resulting distribution. For sample 3, one component for both sites was sufficient, and is related to the low resolution of the spectrum. Notably, the Fe^{3+}/Fe_{tot} ratios obtained by QSD analysis are comparable to those retrieved from Lorentzian site analysis. The uncertainties were calculated using the covariance matrix and errors were estimated no less than ±3% for both Fe^{2+} and Fe^{3+} absorption areas.

X-ray powder diffraction

X-ray powder diffraction (XRPD) data of samples 1 and 2 were collected on a parallel beam Siemens D5005 diffractometer, operating in transmission mode and equipped with a Peltier-cooled Si (Li) detector. XRPD data of samples 3 and 4 were collected on a parallel-beam Bruker AXS D8 Advance diffractometer, operating in transmission mode and equipped with a Position Sensitive Detector (PSD) VÅNTEC-1. Samples were ground in ethanol in an agate mortar and the powders were mounted in a 0.3 mm diameter borosilicate glass capillary. Reasonable compaction was obtained via an ultrasonic cleaner. Preliminary evaluation of diffraction patterns for samples 1 and 2 indicated the presence of albite and, for samples 3 and 4, the presence of albite and sanidine. These minor phases were present in small amounts for samples 1, 2, and 3 (about 10 wt% of albite for samples 1 and 2, about 5 wt% of albite, and 5 wt% of sanidine for sample 3), whereas their amounts were found to be much higher in sample 4 (20 wt% of albite and 10 wt% of sanidine). Rietveld refinements were carried out with the GSAS suite of programs (Larson and Von Dreele 1985) coupled with the EXPGUI graphical interface (Toby 2001). The background was fitted with a 36-term Chebyshev polynomial of the first kind to properly fit the amorphous component from the capillary. Peak-shapes were fitted using the TCH pseudo-Voigt (Thompson et al. 1987) modified for asymmetry (Finger et al. 1994). Refined variables were GV and GW (respectively, tanθ-dependent and angle-independent) Gaussian parameters, LY (tanθ dependent) Lorentzian parameter, and S/L and H/L asymmetry parameters (constrained to be equal in magnitude). Refinement of the scale-factors allowed for a quantitative analysis of the mixture.

Starting structural data of the amphibolic fibers were those of the prismatic fluoro-edenite of Gianfagna and Oberti (2001), whereas those of Meneghinello et al. (1999) and Gualtieri (2000) were, respectively, chosen for the albite and sanidine. Cell parameters, fractional coordinates for all atoms, and site scattering for M1, M2, M3, M4, A, and A(*m*) were refined for the fibers. Moreover, cell parameters were refined for albite and sanidine. Attempts to distribute electron density at the A2 site failed possibly because of correlation with the neighboring A site. Therefore, the simplification of a single site A (special position 0, 0.5, 0) was considered during the refinement. Moreover, for samples 2 and 4, refinements of A and A(*m*) sites also failed.

Isotropic displacement parameters were kept fixed throughout the refinement at the values reported for prismatic fluoro-edenite by Gianfagna and Oberti (2001), because of strong correlations with site occupancies. Restraints on bond distances were imposed as follows: T-O ×8 = 1.635(25) Å, O-O ×12 = 2.67(4) Å, M1-O ×6 = 2.06(2) Å, M2-O ×6 = 2.08(3) Å, M3-O ×6 = 2.05(2) Å, M4-O ×8 = 2.51(20) Å with a weight kept equal to 2 during the refinement, except for sample 4 for which it was required to use a statistical weight of 10 due to the presence of as much as 30% of minor phases in the mixture. Attempts to model the presence of preferred orientation, by means of the generalized spherical harmonics description of Von Dreele (1997), produced a very marginal reduction of the agreement indices as a result of J texture indices close to 1 (Table 2). Experimental and calculated pattern and relative difference for sample 3, for example, is shown in Figure 2. Experimental details and miscellaneous data are shown in Table 2. Fractional coordinates and isotropic displacement for all samples are reported in Table 3. Cell parameters are reported in Table 4, and selected bond distances in Table 5. Notably, the structural data reported here for sample 2 are original and in substantial agreement with those previously reported by Gianfagna et al. (2007). Finally, it must be noted that the

Table 1. ^{57}Fe Mössbauer hyperfine parameters at room temperature (RT) for fibrous amphiboles from Biancavilla; quadrupole splitting distribution (QSD) fitting model

Sample	χ^2	Fe^{2+}				Fe^{3+}				Fe^{3+}_{raw} (% Fe_{tot})	Fe^{3+}_{corr} (% Fe_{tot})
		Δ_0 (mm/s)	σ_Δ (mm/s)	δ_0 (mm/s)	Area (%)	Δ_0 (mm/s)	σ_Δ (mm/s)	δ_0 (mm/s)	Area (%)		
1	0.64	1.89	0.25	1.06	28.2	0.64	0.44	0.38	31.6	59	54
		2.75	0.23	1.06	13.2	1.1	2.2	0.38	27.0		
2*	0.58	1.87	0.28	1.09	18.9	0.77	0.41	0.38	31.4	71	67
		2.65	0.25	1.09	9.7	1.50	1.80	0.38	40.0		
3	0.74	1.96	0.20	0.98	6.9	0.74	0.87	0.35	93.1	93	92
4	0.74	1.93	0.03	1.13	3.1	0.70	0.36	0.35	55.3	95	94
		2.57	0.0	1.13	1.6	1.18	1.31	0.35	40.0		

Notes: Symbols according to Rancourt and Ping (1991): isomer shift (δ_0) with respect to α-iron; δ_1 always lower than 0.05; γ = 0.194 mm/s; h_+/h_- = 1. The Fe^{3+}_{raw} is obtained from the area of absorption peaks assigned to Fe^{3+}. The Fe^{3+}_{corr} is obtained from the raw value by applying the correction factor C = 1.22 (Dyar et al. 1993). Estimated uncertainties are about 0.02 mm/s for hyperfine parameters, and no less than 3% for absorption areas.
* Data from Gianfagna et al. (2007).

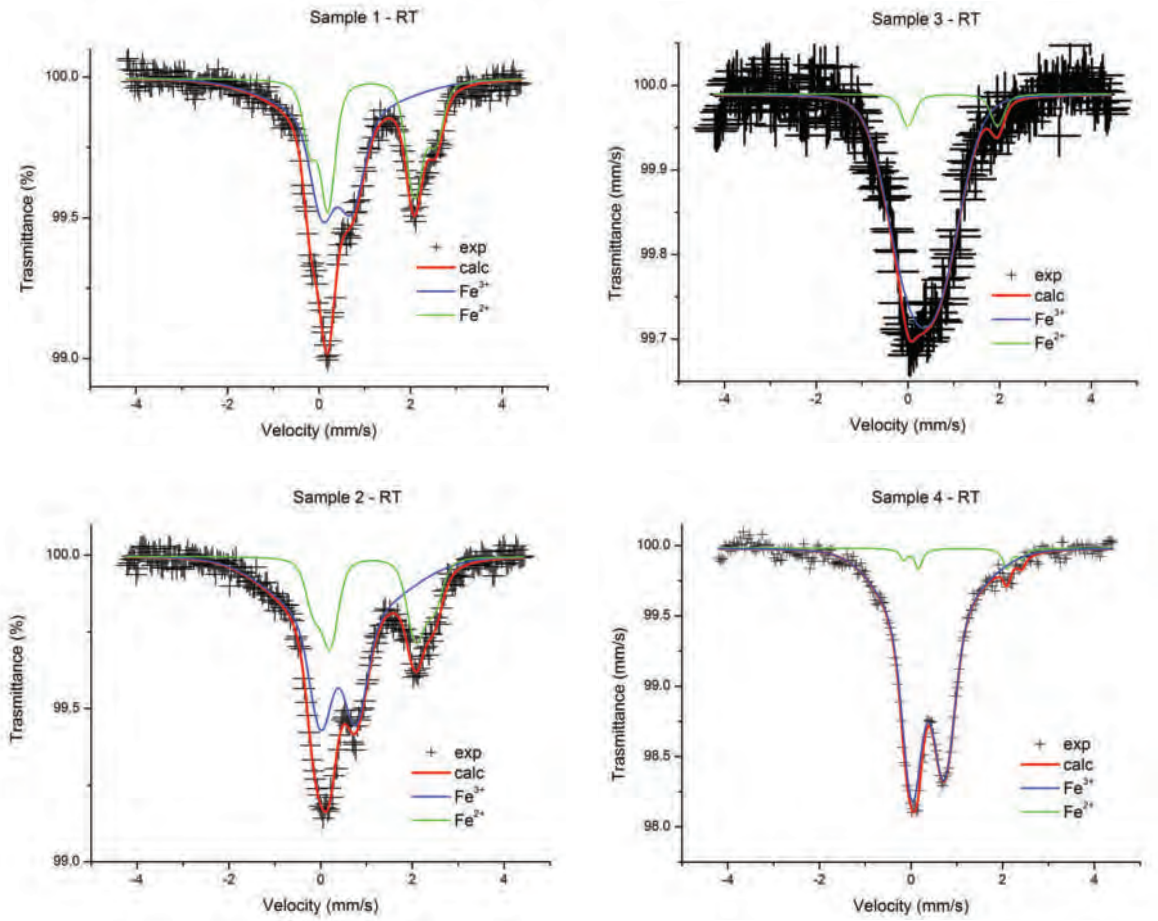

FIGURE 1. Room-temperature (RT) Mössbauer spectra with quadrupole splitting distribution (QSD) fitting model of the four fibrous amphibole samples from Biancavilla.

site scattering and bond distances observed for sample 4 have to be considered less reliable than those of the other samples because of the presence of 30% of feldspars within the analyzed powder. A CIF file is on deposit[1].

RESULTS AND DISCUSSION

Each of the four samples studied is made of loose (not bundled) amphibole fibers, in association with small amounts of feldspars. As specified in Mazziotti-Tagliani et al. (2009), the standardized SEM-EDS chemical analyses were randomly performed on loose fibers (1–3 spots on 40–60 fibers for each sample). Notably, sample 2 is the same sample previously analyzed with the semi-quantitative approach in Gianfagna et al. (2007), and because of this it was reanalyzed. Within each sample, the various fibers show different chemical compositions, ranging from edenite to winchite with variable tremolite component. All samples show nearly parallel compositional trends, which are spaced because of their tremolite component (Fig. 3). In fact, sample 2 shows the highest tremolite content (roughly quantified as ca. 40% on the basis of its average chemical formula), sample

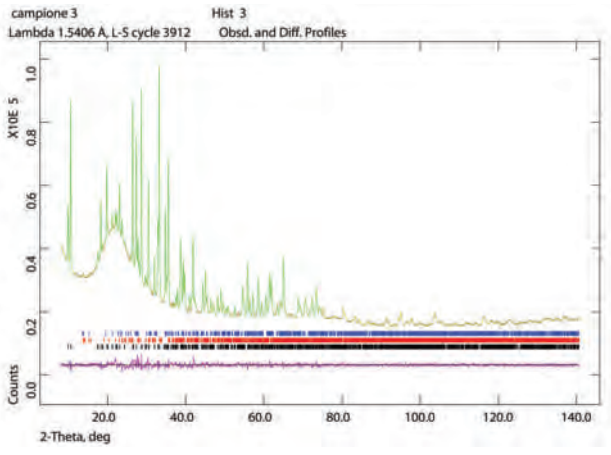

FIGURE 2. Experimental (dots) and calculated (continuous line) Rietveld plots for a fibrous amphibole from Biancavilla (sample 3). Vertical markers refer, from the bottom to the top, to the position of the calculated Bragg reflections for amphibole (in black), albite (in red), and sanidine (in blue). The difference profile is shown at the bottom of the figure.

[1] Deposit item AM-09-047, CIF. Deposit items are available two ways: For a paper copy contact the Business Office of the Mineralogical Society of America (see inside front cover of recent issue) for price information. For an electronic copy visit the MSA web site at http://www.minsocam.org, go to the American Mineralogist Contents, find the table of contents for the specific volume/issue wanted, and then click on the deposit link there.

4 shows an intermediate tremolite content (ca. 30% on the basis of its average chemical formula), and samples 1 and 3 show the lowest tremolite content (ca. 25% on the basis of average chemical formula). However, samples 1 and 3 are different because of their edenite content (ca. 45 and 55%, respectively). Finally, samples 1 and 4 show comparable winchite content (ca. 30%) but different from samples 2 and 3 (ca. 20%). Sample 3 shows the most restricted compositional range.

The average crystal-chemical formulae of the four samples are reported in Table 6. For all samples, small-to-medium amounts of iron (3.6–6.0 wt% FeO_{tot}) were detected by chemical analysis. The Fe^{2+}/Fe^{3+} ratio was quantified by analysis of the Mössbauer spectra. The absorption spectra are typical of paramagnetic materials and are composed of two contributions (Fig. 1). The first one is due to Fe^{2+} components with δ_0 of 1.1 mm/s and a quadrupole splitting centred around Δ_0 of 1.9 and 2.6 mm/s (both in the Lorentzian and in the QSD fits). The second contribution is due to Fe^{3+} components with δ_0 of 0.38 mm/s and a quadrupole splitting distribution, which is sharp at Δ_0 of 0.7 mm/s and very broad between 1.1 and 1.5 mm/s. The Fe^{3+}/Fe_{tot} ratio was quantified from spectral areal measurement (Fe^{3+}_{raw}) and

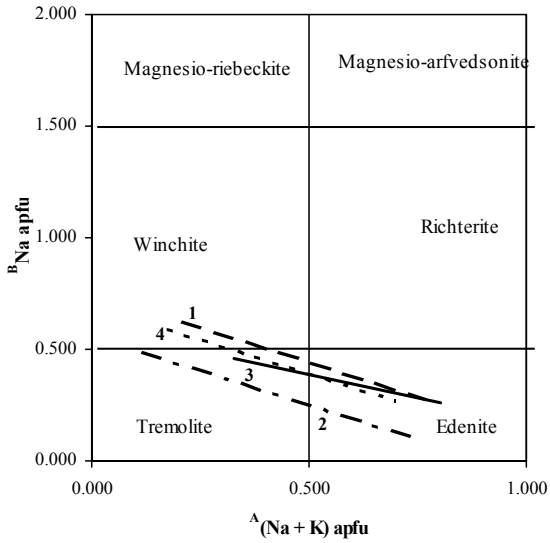

FIGURE 3. Compositional trends retrieved for the four fibrous amphiboles from Biancavilla. Dashed line = sample 1; dashed and dotted line = sample 2; solid line = sample 3; dotted line = sample 4.

TABLE 2. Experimental details of the X-ray power diffraction data collection and miscellaneous data of the refinement for the fibrous amphiboles from Biancavilla

Sample 1	
Instrument	Siemens D5005
X-ray tube	Cu*K*α at 40 kV and 40 mA
Incident beam optic	Multilayer X-ray mirrors
Sample mount	Rotating capillary (30 rpm)
Soller slits	2 (2.3° divergence)
Divergence and antidivergence slits	1 mm
Detector	Solid state Si(Li) SolX
2θ range (°)	5–155
Step size (°)	0.02
Counting time (s)	30
R_p (%); R_{wp} (%); R_F (%)	5.37; 6.27; 4.61
Reduced χ^2	1.35
Restraints contribution to χ^2	185.8
Refined parameters	88
Peak-cut-off (%)	0.5
J	1.005
GV, GW	–5(6), 22(1)
LY	24.3(8)
S/L=H/L	0.0230(7)
Amphibole; albite (wt%)	87.3(1); 12.7(2)
Sample 2*	
Instrument	Siemens D5005
X-ray tube	Cu*K*α at 40 kV and 40 mA
Incident beam optic	Multilayer X-ray mirrors
Sample mount	Rotating capillary (30 rpm)
Soller slits	2 (2.3° divergence)
Divergence and antidivergence slits	1 mm
Detector	Solid state Si(Li) SolX
2θ range (°)	3–120
Step size (°)	0.02
Counting time (s)	30
R_p (%); R_{wp} (%); R_F (%)	5.17; 6.86; 3.93
Reduced χ^2	1.21
Restraints contribution to χ^2	76.1
Refined parameters	92
Peak-cut-off (%)	0.06
J	1.005
GV, GW	18(4), 6.9(7)
LY	18.4(7)
S/L=H/L	0.0231(6)
Amphibole; albite (wt%)	89.0(1); 10.0(4)

* Starting structure of Gianfagna et al. (2007)

TABLE 2.—*CONTINUED*

Sample 3	
Instrument	Bruker AXS D8 Advance
X-ray tube	Cu*K*α at 40 kV and 40 mA
Incident beam optic	Multilayer X-ray mirrors
Sample mount	Rotating capillary (60 rpm)
Soller slits	2 (2.3° divergence + radial)
Divergence and antidivergence slits	0.6 mm
Detector	Position Sensitive Detector (PSD) VÅNTEC-1 opening window 6 °2θ.
2θ range (°)	5–140
Step size (°)	0.02
Counting time (s)	10
R_p (%); R_{wp} (%); R_F (%)	1.02; 1.42; 1.76
Reduced χ^2	4.62
Restraints contribution to χ^2	115.4
Refined parameters	93
Peak-cut-off (%)	0.1
J	1.004
GV, GW	–6(2), 28.9(5)
LY	20.8(3)
S/L=H/L	0.0241(3)
Amphibole; albite; sanidine (wt%)	90.44(2); 5.43(6); 4.13 (7)
Sample 4	
Instrument	Bruker AXS D8 Advance
X-ray tube	Cu*K*α at 40 kV and 40 mA
Incident beam optic	Multilayer X-ray mirrors
Sample mount	Rotating capillary (60 rpm)
Soller slits	2 (2.3° divergence + radial)
Divergence and antidivergence slits	0.6 mm
Detector	Position Sensitive Detector (PSD) VÅNTEC-1 opening window 6 °2θ.
2θ range (°)	5–140
Step size (°)	0.02
Counting time (s)	10
R_p (%); R_{wp} (%); R_F (%)	1.62; 2.17; 1.76
Reduced χ^2	4.62
Restraints contribution to χ^2	690.5
Refined parameters	86
Peak-cut-off (%)	0.2
J	1.008
GV, GW	–46(8), 56(2)
LY	30.0(8)
S/L = H/L	0.0255(7)
Amphibole; albite; sanidine (wt%)	70.7(1); 17.1(1); 12.2(1)

Note: Statistical descriptor as defined by Young (1993).

TABLE 3. Fractional coordinates and isotropic thermal parameters (not refined) for the fibrous amphiboles from Biancavilla

Site	*x*	*y*	*z*	U_{iso} (Å^2)
Sample 1				
O1	0.1105(8)	0.0865(5)	0.2174(17)	0.01
O2	0.1180(10)	0.1703(6)	0.7250(21)	0.01
O3	0.1014(12)	0	0.7090(20)	0.01
O4	0.3681(12)	0.2477(4)	0.7997(24)	0.01
O5	0.3459(12)	0.1328(5)	0.0976(17)	0.01
O6	0.3442(12)	0.1139(5)	0.5987(17)	0.01
O7	0.3451(16)	0	0.2745(31)	0.01
T1	0.2772(6)	0.08347(29)	0.2926(11)	0.005
T2	0.2917(4)	0.16898(29)	0.8050(12)	0.005
M1	0	0.0884(53)	0.5	0.006
M2	0	0.1770(4)	0	0.006
M3	0	0	0	0.006
M4	0	0.27571(35)	0.5	0.011
A	0	0.5	0	0.025
Sample 2				
O1	0.1109(10)	0.0850(6)	0.2225(21)	0.01
O2	0.1186(12)	0.1722(7)	0.7215(25)	0.01
O3	0.1048(13)	0	0.7092(25)	0.01
O4	0.3661(14)	0.2486(5)	0.7914(29)	0.01
O5	0.3475(15)	0.1342(6)	0.0990(22)	0.01
O6	0.3443(14)	0.1162(6)	0.5968(22)	0.01
O7	0.3431(18)	0	0.289(4)	0.01
T1	0.2794(7)	0.08388(35)	0.2957(15)	0.005
T2	0.2916(8)	0.17076(35)	0.8052(15)	0.005
M1	0	0.0882(5)	0.5	0.006
M2	0	0.1768(5)	0	0.006
M3	0	0	0	0.006
M4	0	0.2762(4)	0.5	0.011
A	0	0.5	0	0.020
A(*m*)	0.082(14)	0.5	0.079(22)	0.030
Sample 3				
O1	0.1121(5)	0.08488(21)	0.2196(8)	0.01
O2	0.1168(5)	0.17076(23)	0.7279(8)	0.01
O3	0.1016(4)	0	0.7136(10)	0.01
O4	0.3614(5)	0.24898(18)	0.7982(11)	0.01
O5	0.3492(6)	0.13333(19)	0.1006(9)	0.01
O6	0.3434(5)	0.11831(20)	0.5983(10)	0.01
O7	0.3454(6)	0	0.2830(13)	0.01
T1	0.28044(25)	0.08421(11)	0.2971(5)	0.005
T2	0.28837(28)	0.17102(10)	0.8057(5)	0.005
M1	0	0.08670(16)	0.5	0.006
M2	0	0.17833(15)	0	0.006
M3	0	0	0	0.006
M4	0	0.27751(13)	0.5	0.011
A	0	0.5	0	0.020
A(*m*)	0.0443(29)	0.5	0.131(8)	0.030
Sample 4				
O1	0.1100(7)	0.0857(4)	0.2205 (14)	0.01
O2	0.1142(8)	0.1733 (4)	0.7190(17)	0.01
O3	0.1048(9)	0	0.7177(16)	0.01
O4	0.3614(10)	0.24980(34)	0.8014(19)	0.01
O5	0.3497(10)	0.1327(4)	0.0931(14)	0.01
O6	0.3427(10)	0.1195(4)	0.5938(14)	0.01
O7	0.3462(12)	0	0.2874(24)	0.01
T1	0.2780(5)	0.08468(22)	0.2939(9)	0.005
T2	0.2906(6)	0.17007(23)	0.8080(9)	0.005
M1	0	0.08645(35)	0.5	0.006
M2	0	0.17903(29)	0	0.006
M3	0	0	0	0.006
M4	0	0.27827(31)	0.5	0.011
A	0	0.5	0	0.025

corrected by applying the correction factor of Dyar et al. (1993). The final, corrected Fe^{3+}/Fe_{tot} ratios (Fe^{3+}_{corr}) were 54 and 67% Fe_{tot} for samples 1 and 2, respectively, and 92 and 94% Fe_{tot} for samples 3 and 4, respectively (Table 1).

In agreement with the literature, Fe^{2+} was primarily assigned to an irresolvable combinations of M1+M3 sites, represented by the component with Δ_0 of 2.6 mm/s, and M2+M4 sites, represented by the component with Δ_0 of 1.9 mm/s. This is not in contrast with the cation site-partition based on XRPD data (Table 7). In fact, in all cases (except sample 3 in which the two Mössbauer components were not refined), the amount of Fe^{2+} assigned to M2+M4 is almost twice than that assigned to M1+M3. The two Fe^{3+} components are more difficult to explain. On the basis of reference data, Fe^{3+} should be ordered at M2, as observed for sodic amphiboles (Ernst and Wai 1970), strontian potassic-richterite (Sokolova et al. 2000), ferrian winchite (Sokolova et al. 2001), winchite-richterite (Gunter et al. 2003), fluoro-edenite (Gianfagna et al. 2007), and fibrous tremolite (Ballirano et al. 2008). Accordingly, we have assigned most of the Fe^{3+} to the M2 site. The additional, broad component observed in our spectra at 1.1–1.5 mm/s, which is modeled by a large quadrupole splitting distribution, could be due to many different factors. As suggested by Gunter et al. (2003), it could be caused by crystal size or isolated magnetic states for Fe^{3+}. Alternatively, this broad component could be related to Fe^{3+} disorder over different octahedra (as in sample 4; see Table 7) or even to other cations locally disordered around Fe^{3+} (as in sample 2; see Table 7), as commonly observed in complex silicates (Andreozzi et al. 2004, 2008).

TABLE 4. Unit-cell parameters obtained for the fibrous amphiboles from Biancavilla

	a (Å)	*b* (Å)	*c* (Å)	β(°)	*V* (Å^3)
1	9.8056(4)	18.0105(7)	5.2725(2)	104.406(3)	901.86(6)
2	9.8112(3)	18.0162(6)	5.2774(2)	104.624(2)	902.61(5)
3	9.8272(1)	17.9899(2)	5.2756(1)	104.596(1)	902.57(2)
4	9.7935(3)	17.9728(5)	5.2746(1)	104.403(2)	899.23(5)
F-edenite 2003	9.8445(3)	18.0091(6)	5.2772(2)	104.813(2)	904.50(5)
F-edenite 2001	9.846(4)	18.009(6)	5.277(2)	104.77(2)	904.8(5)

Note: Cell parameters of prismatic fluoro-edenite obtained from powder analysis (Gianfagna et al. 2003) and those obtained from single-crystal analysis (Gianfagna and Oberti 2001) are reported for comparison.

Structural data and site scattering (s.s.) values are reported in Tables 4, 5, and 7. Sample 4 shows the smallest *a* and *b* cell parameters, and this is consistent with its highest Fe^{3+} content in C sites. In the fibrous samples, the *c* cell-parameter is directly related to tetrahedral Al content (Table 6). The main difference with respect to prismatic fluoro-edenite is the general reduction of some of the cell parameters: in particular, *a* (9.794–9.827 Å for the fibers and 9.846 Å for the prismatic fluoro-edenite), β (104.40–104.62° for the fibers and 104.77° for the prismatic fluoro-edenite) and, consequently, cell volume (900–902 Å^3 for the fibers and 904 Å^3 the prismatic fluoro-edenite). The reduction of the *a* cell parameter is consistent with the smaller A-site occupancy, and the reduction of β angle is consistent with the smaller Ca content (Table 6). Within all samples, the refined <T-O> and <M-O> distances may be considered statistically equal (within their uncertainties). However, sample 2 shows the largest <M-O> value (2.067 Å compared with 2.057–2.060 Å of the other samples), in agreement with its highest Fe^{2+} content.

For each sample, calculated total site scattering (corresponding to the sum of electrons per formula unit) was derived from chemical data integrated by Mössbauer analysis. Possible site occupancy was obtained by combining integrated chemical data with Rietveld refinement results (Table 7). Good agreement is observed between the s.s. refined values and those calculated from the possible site occupancy (Table 7). The largest differ-

ences, observed for C sites, are smaller than 3% relative.

Samples 2 and 4 show refined s.s. values at C sites higher than those for samples 1 and 3. This is due to the larger amounts of heavier atoms (e.g., Fe). In particular, since the refined s.s. at M1 and M3 sites are not significantly different within all samples, the observed increase of s.s. at C sites is mainly due to the presence of both Fe^{2+} and Fe^{3+} at M2 site, and just marginally to the presence of either Fe^{2+} (samples 1 and 2) or Fe^{3+} (samples 3 and 4) at M1 site. Moreover, all fibrous samples show s.s. values at C sites higher than the prismatic fluoro-edenite, as a consequence of their highest (Fe^{2+}+Fe^{3+}) content. For all samples, with the exception of sample 1, the <M4-O> distances are randomly distributed (within their uncertainties) around the value of prismatic fluoro-edenite. For sample 1, the largest distance is consistent with the highest content of Na at M4 site. The refined s.s. values of M4 site are in good agreement with those calculated, the largest difference being smaller than 3% relative for all samples but sample 4. The latter shows a difference of 10% relative, due to abundant accessory phases. Samples 1 and 2 show s.s. values of M4 very close to that of prismatic fluoro-edenite (37.18) and larger than those of the samples 3 and 4. Notably, for samples 1 and 2, the high s.s. value is not justified by a high Ca content, but by Fe^{2+} content (Table 7). In fact, the site partition for these samples allowed us to decipher the combination of irresolvable $^{M2+M4}Fe^{2+}$ observed by Mössbauer spectroscopy, and to reveal that Fe^{2+} is equally distributed or preferentially ordered at M4.

Finally, all samples show statistically equal <A-O> and <A(*m*)-O> distances. The s.s. values of fibrous samples are significantly lower than that of the prismatic fluoro-edenite, and this is related to the lowest content of ^{A}Na in the fibers.

Environmental and health relevance

In the case of Biancavilla, the environmental and medical relevance of the amphibole fibers was clearly evidenced by previous studies. However, questions remained about fiber classification, their reactivity, and the mechanisms of biochemical fiber/tissues interactions, including the quantification of the minimal inhaled dose (triggering dose).

In this study, we observed that the mineral fibers have a composition ranging from fluoro-edenite [$NaCa_2Mg_5Si_7AlO_{22}F_2$] to winchite [$\square NaCaMg_4(Al,Fe^{3+})Si_8O_{22}(OH)_2$], with variable tremolite [$\square Ca_2(Mg,Fe^{2+})_5Si_8O_{22}(OH)_2$] component. The compositional variation of single fibers is extremely wide: as for example, according to the Leake et al. (1997) classification, sample 2 would have more than 50% of its fibers plotting in the tremolite field, samples 1 and 3 would have more than 50% of their fibers plotting in the edenite field, and sample 4 would have almost the same amount of fibers plotting in the tremolite and winchite fields. Consequently, classification of the fibers is very difficult and the definition of mineral species names almost impossible. Furthermore, in spite of their morphologies, compositions, and recognized dangers, the fibers from Biancavilla are not regulated as "asbestos." In fact, among amphibole fibers previously mentioned, the regulatory agencies classify the fibrous tremolite as "asbestos," but do not classify the whole mineral series as asbestos. The fibrous amphiboles from Biancavilla therefore represent a case of environmental pollution from natural mineral fibers, due to non-occupational exposure. A similar case was reported by Gunter et al. (2003) for the amphibole fibers from Libby,

Table 6. Average crystal-chemical formulae of the fibrous amphiboles from Biancavilla

	1	2	3	4	F-edenite 2001
Si	7.676	7.495	7.544	7.587	7.317
^{IV}Al	0.324	0.488	0.418	0.384	0.638
Σ*T*	8.000	7.984	7.962	7.971	7.955
^{VI}Al	0.002	0.000	0.000	0.000	0.000
Ti	0.003	0.004	0.002	0.003	0.030
Fe^{3+}	0.348	0.477	0.390	0.557	0.271
Mg	4.511	4.350	4.758	4.607	4.749
Fe^{2+}	0.296	0.235	0.034	0.036	0.020
Mn	0.067	0.055	0.059	0.053	0.047
Σ*C*	5.227	5.121	5.243	5.256	5.117
Δ*C*	0.227	0.121	0.243	0.256	0.117
Ca	1.289	1.555	1.389	1.297	1.627
Na	0.484	0.324	0.368	0.447	0.256
Σ*B*	2.000	2.000	2.000	2.000	2.000
Na	0.368	0.307	0.474	0.312	0.584
K	0.096	0.094	0.099	0.097	0.159
Σ*A*	0.462	0.401	0.573	0.409	0.743
F	1.974	1.981	1.963	1.961	1.977
Cl	0.014	0.014	0.014	0.014	0.019
ΣO_3	1.988	1.995	1.977	1.975	1.996
^{B}Na	0.484	0.325	0.368	0.447	0.257
^{A}(Na+K)	0.462	0.400	0.573	0.409	0.741

Notes: Fe^{2+}/Fe^{3+} ratios from Mössbauer spectroscopy. Crystal-chemical formula of the prismatic fluoro-edenite (Gianfagna and Oberti 2001) is shown for comparison.

Table 5. Selected bond distances (Å) for the fibrous amphiboles from Biancavilla

Sample	1	2	3	4	F-edenite 2001	Sample	1	2	3	4	F-edenite 2001
T1-O1	1.585(8)	1.600(10)	1.601(4)	1.594(7)	1.624(1)	T2-O4	1.607(8)	1.592(9)	1.581(4)	1.596(6)	1.589(1)
T1-O7	1.656(7)	1.639(8)	1.653(3)	1.666(5)	1.635(1)	T2-O2	1.650(8)	1.643(10)	1.632(4)	1.675(7)	1.621(1)
T1-O5	1.626(8)	1.642(10)	1.633(4)	1.651(7)	1.645(1)	T2-O6	1.646(8)	1.653(10)	1.639(4)	1.628(6)	1.670(1)
T1-O6	1.676(8)	1.661(11)	1.670(5)	1.672(5)	1.643(2)	T2-O5	1.637(9)	1.646(11)	1.664(5)	1.617(8)	1.655(5)
<T1-O>	1.636	1.636	1.639	1.646	1.637	<T2-O>	1.635	1.634	1.629	1.629	1.634
M1-O3 ×2	2.047(7)	2.057(9)	2.033(3)	2.049(6)	2.059(1)	M2-O4 ×2	1.987(10)	2.003(12)	1.992(5)	1.967(8)	2.003(1)
M1-O1 ×2	2.049(8)	2.034(10)	2.055(4)	2.030(7)	2.056(1)	M2-O2 ×2	2.071(9)	2.094(11)	2.056(4)	2.070(8)	2.080(1)
M1-O2 ×2	2.059(9)	2.079(11)	2.087(5)	2.092(7)	2.062(1)	M2-O1 ×2	2.127(9)	2.158(11)	2.177(4)	2.168(8)	2.152(1)
<M1-O>	2.051	2.057	2.058	2.057	2.059	<M2-O>	2.062	2.085	2.075	2.068	2.078
M3-O3 ×2	2.025(9)	2.052(11)	2.010(4)	1.995(8)	2.029(2)	M4-O4 ×2	2.316(12)	2.305(14)	2.374(5)	2.387(9)	2.336(1)
M3-O1 ×4	2.073(8)	2.064(10)	2.060(4)	2.067(8)	2.055(1)	M4-O2 ×2	2.381(11)	2.355(14)	2.399(5)	2.346(9)	2.419(1)
						M4-O6 ×2	2.637(11)	2.597(13)	2.560(4)	2.525(9)	2.550(2)
<M3-O>	2.058	2.060	2.043	2.043	2.046	M4-O5 ×2	2.811(11)	2.779(14)	2.763(5)	2.786(9)	2.743(2)
<A-O>	3.03	3.06	3.05	3.05	2.926	<M4-O>	2.536	2.509	2.524	2.511	2.512
<A(*m*)-O>	–	3.02	2.87	–	2.863						

Note: Selected bond distances of prismatic fluoro-edenite obtained from single-crystal analysis (Gianfagna and Oberti 2001) are reported for comparison.

Montana. Fibers in Libby were recognized to be a solid-solution series with compositions ranging from winchite to richterite. In both localities, amphibole fibers in altered volcanic products, mined for commercial purposes, were recognized as the cause of the anomalously high incidence of malignant mesothelioma in miners and/or local inhabitants. In spite of the very different compositional trends shown by Libby and Biancavilla fibers, their average Fe contents and oxidation states are similar. It is well known that the presence of Fe in mineral fibers, particularly in the Fe^{2+} oxidation state, may cause carcinogenesis by participating in Fenton chemistry, that is, producing reactive oxygen species (ROS), which determines a strong release of •OH free radicals (Kane et al. 1996; Fubini and Otero Aréan 1999; Kamp and Weitzman 1999; Robledo and Mossman 1999). Moreover, it has been suggested by Shulka et al. (2003) that the bioactivity of Fe is dependent on its coordination environment in the structure. The Fe topochemistry in amphibole fibers was recently addressed by Ballirano et al. (2008), who focused on Fe content, Fe^{2+}-Fe^{3+} speciation and site distribution in the structure of an Fe-bearing fibrous tremolite from the Susa Valley (Piedmont, Italy). Such fibers, notwithstanding their low Fe content (FeO_{tot} ca. 1 wt%), showed very low Fe^{3+}/Fe_{tot} ratios, and had been found to be very dangerous indeed, since they caused generation of ROS, induction of cell oxidative stress, and inhibition of anti-oxidative defenses (Turci et al. 2007).

As reported in Mazziotti-Tagliani et al. (2009), Biancavilla single fibers show FeO_{tot} contents spanning a range from ca. 2 to ca. 7 wt%. Furthermore, every sample displays large chemical heterogeneity, but sample 3 has, on average the lowest FeO_{tot} content, and samples 1 and 2 have the lowest Fe^{3+}/Fe_{tot} ratios (Table 1). Recent biological in vitro tests on two samples of Biancavilla fibers confirmed their high reactivity via the induction of cell oxidative stress and inflammatory response and, therefore, their dangerousness (Cardile et al. 2007). Moreover, preliminary results of toxicological tests [MTT (cytotoxicity) tests on A549 and MeT-5A cells] on exactly the same four samples studied here suggest that the sample 3 induced the lowest cellular toxicity (A. Pugnaloni, personal communication) although did not exhibit large differences (within experimental error) of cell mortality among the various samples. Notably, a rapid start of cell mortality was observed for samples 1 and 2, whereas a delay was observed for samples 3 and 4, which, recall, are the samples with the highest Fe^{3+}/Fe_{tot} ratios. This is consistent with the Fe-catalyzed Haber-Weiss cycle in which the Fe^{3+} must be previously reduced to Fe^{2+} to produce ROS (Fubini and Otero Aréan 1999). Due to the results obtained thus far (and the environmental and health relevance of the topic), further studies are in progress on the same samples, concerning the characterization of the fiber surface chemistry (focused on Fe oxidation state) and reactivity (detection of oxy-radicals and monitoring of lipid peroxidation).

TABLE 7. Site scattering (s.s.) values for the fibrous amphiboles: experimentally obtained from the structural refinement (left); calculated from the possible site occupancy (right)

	s.s. from refinement	Possible site occupancy	s.s. from site occupancy
Sample 1			
A	4.6(2)	$K_{0.10}Na_{0.37}$	6.0
A(*m*)	–	–	–
Sum *A* sites	4.6(2)		6.0
M4	37.6(4)	$Ca_{1.29}Na_{0.48}Mn^{2+}_{0.07}Fe^{2+}_{0.16}$	37.0
Sum *B* sites	37.6(4)		37.0
M1	25.0(3)	$Mg_{1.90}Fe^{2+}_{0.10}$	25.3
M2	28.0(3)	$Mg_{1.61}Fe^{2+}_{0.04}Fe^{3+}_{0.35}$	29.5
M3	11.8(2)	$Mg_{1.00}$	12.0
Sum *C* sites	64.8(5)		66.8
Sample 2			
A	2.9(8)	$K_{0.09}$	1.7
A(*m*)	3.3(8)	$Na_{0.31}$	3.4
Sum *A* sites	6.2(11)		5.1
M4	37.3(4)	$Ca_{1.56}Na_{0.32}Mn^{2+}_{0.05}Fe^{2+}_{0.07}$	37.8
Sum *B* sites	37.3(4)		37.8
M1	25.3(4)	$Mg_{1.92}Fe^{2+}_{0.08}$	25.1
M2	30.6(4)	$Mg_{1.44}Fe^{2+}_{0.08}Fe^{3+}_{0.48}$	31.8
M3	12.2(3)	$Mg_{0.99}Fe^{2+}_{0.01}$	12.1
Sum *C* sites	68.1(6)		69.0
Sample 3			
A	3.3(3)	$K_{0.10}$	1.9
A(*m*)	4.4(3)	$Na_{0.47}$	5.2
Sum *A* sites	7.7(4)		7.1
M4	34.1(1)	$Ca_{1.39}Na_{0.37}Mn^{2+}_{0.06}Mg_{0.18}$	35.5
Sum *B* sites	34.1(1)		35.5
M1	25.3(1)	$Mg_{1.87}Fe^{3+}_{0.12}$	25.6
M2	27.7(1)	$Mg_{1.70}Fe^{2+}_{0.03}Fe^{3+}_{0.27}$	28.2
M3	11.8(1)	$Mg_{1.00}$	12.0
Sum *C* sites	64.8(2)		65.8
Sample 4			
A	6.8(2)	$K_{0.10}Na_{0.31}$	5.3
A(*m*)	–	–	–
Sum *A* sites	6.8(2)		5.3
M4	30.8(3)	$Ca_{1.30}Na_{0.45}Mn^{2+}_{0.05}Mg_{0.20}$	34.6
Sum *B* sites	30.8(3)		34.6
M1	24.1(2)	$Mg_{1.96}Fe^{3+}_{0.04}$	24.6
M2	30.3(2)	$Mg_{1.48}Fe^{2+}_{0.04}Fe^{3+}_{0.48}$	31.3
M3	12.7(2)	$Mg_{0.96}Fe^{3+}_{0.04}$	12.6
Sum *C* sites	67.1(5)		68.5

Note: The possible site occupancy is the result of combining data from averaged chemical composition, Mössbauer spectroscopy, and Rietveld refinement.

ACKNOWLEDGMENTS

A. Maras is gratefully thanked for FTIR data collection and interpretation. Constructive revision of M.E. Gunter and D.M. Jenkins, and careful handling by Associate Editor M.D. Dyar greatly improved the clearness of the manuscript.

REFERENCES CITED

Andreozzi, G.B., Lucchesi, S., Graziani, G., and Russo, U. (2004) Site distribution of Fe^{2+} and Fe^{3+} in axinite mineral group: the new crystal-chemical formula. American Mineralogist, 89, 1763–1771.

Andreozzi, G.B., Bosi, F., and Longo, M. (2008) Linking Mössbauer and structural parameters in elbaite-schorl-dravite tourmalines. American Mineralogist, 93, 658–666.

Ballirano, P., Andreozzi, G.B., and Belardi, G. (2008) Crystal chemical and structural characterization of fibrous tremolite from Susa Valley, Italy, with comments on potential harmful effects on human health. American Mineralogist, 93, 1349–1355.

Bruni, B.M., Pacella, A., Mazziotti-Tagliani, S., Gianfagna, A., and Paoletti, L. (2006) Nature and extent of the exposure to fibrous amphiboles in Biancavilla. Science of the Total Environment, 370, 9–16.

Burragato, F., Comba, P., Baiocchi, V., Palladino, D.M., Simei, S., Gianfagna, A., Paoletti, L., and Pasetto, R. (2005) Geo-volcanological, mineralogical and environmental aspects of quarry materials related to pleural neoplasm in the area of Biancavilla, Mount Etna (Eastern Sicily, Italy). Environmental Geology, 47, 855–868.

Cardile, V., Renis, M., Scifo, C., Lombardo, L., Gulino, R., Mancari, B., and Panico, A.M. (2004) Behaviour of new asbestos amphibole fluoro-edenite in different lung cell systems. The International Journal of Biochemistry and Cell Biology, 36, 849–860.

Cardile, V., Lombardo, L., Belluso, E., Panico, A.M., Renis, M., Gianfagna, A., and Balazy, M. (2007) Fluoro-edenite fibers induce expression of Hsp70 and inflammatory response. International Journal of Environmental Research and Public Health, 4, 195–202.

Comba, P., Gianfagna, A., and Paoletti, L. (2003) The pleural mesothelioma cases in Biancavilla are related to the new fluoro-edenite fibrous amphibole. Archives of Environmental and Occupational Health, 58, 229–232.

Dyar, M.D., Mackwell, S.M., McGuire, A.V., Cross, L.R., and Robertson, J.D. (1993) Crystal chemistry of Fe^{3+} and H^{+} in mantle kaersutite: Implications for mantle metasomatism. American Mineralogist, 78, 968–979.

Ernst, W.G. and Wai, C.N. (1970) Mössbauer, infrared, X-ray and optical study of cation ordering and dehydrogenation in natural and heat-treated sodic amphiboles. American Mineralogist, 55, 1226–1258.

Finger, L.W., Cox, D.E., and Jephcoat, A.P. (1994) A correction for powder diffraction peak asymmetry due to axial divergence. Journal of Applied Crystallography, 27, 892–900.

Fubini, B. and Otero Aréan, C. (1999) Chemical aspects of the toxicity of inhaled mineral dusts. Chemical Society Reviews, 28, 373–381.

Gianfagna, A. and Oberti, R. (2001) Fluoro-edenite from Biancavilla (Catania, Sicily, Italy): Crystal chemistry of a new amphibole end-member. American Mineralogist, 83, 1486–1493.

Gianfagna, A., Ballirano, P., Bellatreccia, F., Bruni, B.M., Paoletti, L., and Oberti, R. (2003) Characterization of amphibole fibers linked to mesothelioma in the area of Biancavilla, Eastern Sicily, Italy. Mineralogical Magazine, 67, 1221–1229.

Gianfagna, A., Andreozzi, G.B., Ballirano, P., Mazziotti-Tagliani, S., and Bruni, B.M. (2007) Structural and chemical contrasts between prismatic and fibrous fluoro-edenite from Biancavilla, Sicily, Italy. Canadian Mineralogist, 45, 249–262.

Gualtieri, A.F. (2000) Accuracy of XRPD QPA using the combined Rietveld-RIR method. Journal of Applied Crystallography, 33, 267–278.

Gunter, M.E., Dyar, M.D., Twamley, B., Foit Jr., F.F., and Cornelius, C. (2003) Composition, $Fe^{3+}/\Sigma Fe$, and crystal structure of non-asbestiform and asbestiform amphiboles from Libby, Montana, U.S.A. American Mineralogist, 88, 1970–1978.

Gunter, M.E., Sanchez, M.S., and Williams, T.J. (2007) Characterization of chrysotile samples for the presence of amphiboles: the Carey Canadian deposit, southeastern Quebec, Canada. Canadian Mineralogist, 45, 263–280.

Kamp, D.W. and Weitzman, S.A. (1999) The molecular basis of asbestos induced lung injury. Thorax, 54, 638–652.

Kane, A.B., Boffetta, P., and Wilbourn, J.D. (1996) Mechanisms of Fibre Carcinogenesis. IARC Scientific Publication 140, Lyon, France.

Lagarec, K. and Rancourt, D.G. (1998) RECOIL. Mössbauer spectral analysis software for Windows, version 1.0. Department of Physics, University of Ottawa, Canada.

Larson, A.C. and Von Dreele, R.B. (1985) General Structure Analysis System (GSAS). Los Alamos National Laboratory Report LAUR 86-748.

Leake, B.E., Woolley, A.R., Arps, C.E.S., Birch, W.D., Gilbert, M.C., Grice, J.D., Hawthorne, F.C., Kato, A., Kisch, H.J., Krivovichev, V.G., Linthout, K., Laird, J., Mandarino, J.A., Maresch, V.W., Nickel, E.H., Rock, N.M.S., Schumacher, J.C., Smith, D.C., Stephenson, N.N., Ungaretti, L., Whittaker, E.J.W., and Youzhi, G. (1997) Nomenclature of amphiboles: report of the subcommittee on amphiboles of the International Mineralogical Association, Commission on New Minerals and Mineral Names. American Mineralogist, 82, 1019–1037.

Long, G.J., Cranshaw, T.E., and Longworth, G. (1983) The ideal Mössbauer effect absorber thickness. Mössbauer Effect Reference Data Journal, 6, 42–49.

Mazziotti-Tagliani, S., Andreozzi, G.B., Bruni, B.M., Gianfagna, A., Pacella, A., and Paoletti, L. (2009) Chemical variability of a suite of fibrous amphiboles from Biancavilla (Sicily, Italy). Periodico di Mineralogia, 78, 65–74.

Meeker, G.P., Bern, A.M., Brownfield, I.K., Lowers, H.A., Sutley, S.J., Hoefen, T.M., and Vance, J.S. (2003) The composition and morphology of amphiboles from the Rainy Creek Complex, near Libby, Montana. American Mineralogist, 88, 1955–1969.

Meneghinello, E., Alberti, A., and Cruciani, G. (1999) Order-disorder process in the tetrahedral sites of albite. American Mineralogist, 84, 1144–1151.

Pacella, A., Andreozzi, G.B., Ballirano, P., and Gianfagna, A. (2008) Crystal chemical and structural characterization of fibrous tremolite from Ala di Stura (Lanzo Valley, Italy). Periodico di Mineralogia, 77, 51–62.

Paoletti, L., Batisti, D., Bruno, C., Di Paola, M., Gianfagna, A., Mastrantonio, M., Nesti, M., and Comba, P. (2000) Unusually high incidence of malignant pleural mesothelioma in a town of the eastern Sicily: an epidemiological and environmental study. Archives of Environmental and Occupational Health, 55, 392–398.

Paoletti, L., Bruni, B.M., Arrizza, L., Mazziotti-Tagliani, S., and Pacella, A. (2008) A micro-analytical SEM-EDS method applied to the quantitative chemical compositions of fibrous amphiboles. Periodico di Mineralogia, Special Issue, 77, 63–73.

Pugnaloni, A., Lucarini, G., Giantomassi, F., Lombardo, L., Capella, S., Belluso, E., Zizzi, A., Panico, A.M., Biagini, G., and Cardile, V. (2007) In vitro study of biofunctional indicators after exposure to asbestos-like fluoro-edenite fibres. Cellular and Molecular Biology, 53, 965–80.

Rancourt, D.G. and Ping, J.Y. (1991) Voigt–based methods for arbitrary-shape static hyperfine parameter distributions in Mössbauer spectroscopy. Nuclear Instruments and Methods in Physics Research, B58, 85–97.

Robledo, R. and Mossman, R. (1999) Cellular and molecular mechanisms of asbestos-induced fibrosis. Journal of Cellular Physiology, 180, 158–166.

Shukla, A., Gulumian, M., Hei, T.K., Kamp, D., Rahman, Q., and Mossman, B.T. (2003) Serial review: role of reactive oxygen and nitrogen species (ROS/XRNS) in lung injury and diseases. Multiple roles of oxidants in the pathogenesis of asbestos–induced diseases. Free Radical Biology and Medicine, 34, 1117–1129.

Soffritti, M., Minardi, F., Bua, L., Degli Esposti, D., and Belpoggi, F. (2004) First experimental evidence of peritoneal and pleural mesotheliomas induced by fluro-edenite fibres in Etnean volcanic material from Biancavilla (Sicily, Italy). European Journal of Oncology, 9, 169–175.

Sokolova, E.V., Kabalov, Y.K., McCammon, C., Schneider, J., and Konev, A.A. (2000) Cation partitioninig in an unusual strontian potassicrichterite from Siberia: Rietveld structure refinement and Mössbauer spectroscopy. Mineralogical Magazine, 64, 19–23.

Sokolova, E.V., Hawthorne, F.C., McCammon, C., and Schneider, J. (2001) Ferrian winchite from the Ilmen Mountains, Southern Urals, Russia and some problems with the current scheme of nomenclature. Canadian Mineralogist, 39, 171–177.

Thompson, P., Cox, D.E., and Hastings, J.B. (1987) Rietveld refinement of Debye-Scherrer synchrotron X–ray data from Al_2O_3. Journal of Applied Crystallography, 20, 79–83.

Toby, B.H. (2001) EXPGUI, a graphical user interface for GSAS. Journal of Applied Crystallography, 34, 210–213.

Turci, F., Gazzano, E., Tomatis, M., Riganti, C., Ghigo, D., and Fubini, B. (2007) La tremolite nelle alpi occidentali: un'analisi chimico-fisica con prospettive tossicologiche. Workshop "Anfiboli fibrosi: nuove problematiche relative al rischio ambientale e sanitario." Roma, 27–28 April 2007, Abstracts, 68–72 (in Italian).

Von Dreele, R.B. (1997) Quantitative texture analysis by Rietveld refinement. Journal of Applied Crystallography, 30, 517–525.

Young, R.A. (1993) Introduction to the Rietveld method. In R.A. Young, Ed., The Rietveld Method, p. 1–38. Oxford Science, U.K.

Manuscript received February 9, 2009
Manuscript accepted June 16, 2009
Manuscript handled by M. Darby Dyar